Article

Efficient Removal of Tetracycline by Metal–Organic Framework ZIF-67 and Its Mechanism

Shengyang Zheng [1], Yaping Xu [1], Xu Yao [1,2], Chenzhe Wang [1], Ping Liu [1], Haitao Zhao [1], Jianbing Lu [1] and Jing Ju [1,*]

[1] College of Environmental Science and Engineering/Key Laboratory of Cultivated Land Quality Monitoring and Evaluation, Ministry of Agriculture and Rural Affairs/Jiangsu Collaborative Innovation Center for Solid Organic Waste Resource Utilization, Yangzhou University, Yangzhou 225127, China; syzheng@yzu.edu.cn (S.Z.); mz120221296@stu.yzu.edu.cn (Y.X.); yx18861115577yaoxu@163.com (X.Y.); mx120210702@stu.yzu.edu.cn (C.W.); liuping329098@163.com (P.L.); htzhao@yzu.edu.cn (H.Z.); yzsljb2003@126.com (J.L.)

[2] Jiangsu Longhuan Environmental Technology Co., Ltd., Changzhou 225127, China

* Correspondence: jujing@yzu.edu.cn

Abstract: The widespread use of tetracycline (TC) poses potential hazards to ecosystems and human health. In this study, ZIF-67 was successfully synthesized using a room-temperature static synthesis method and applied to the efficient removal of TC from water. It was shown that the maximum adsorption of TC by ZIF-67 could reach $1583.128 \text{ mg} \cdot \text{g}^{-1}$ at pH = 5.0, an initial TC concentration of $450 \text{ mg} \cdot \text{g}^{-1}$, an adsorption time of 720 min, and a temperature of 308K. The pseudo-second-order kinetic model and Langmuir's isothermal adsorption model could describe the adsorption process better, which proved that the adsorption of ZIF-67 on TC was mainly monolayer adsorption dominated by chemisorption. Mechanistic studies showed that the adsorption process of ZIF-67 on TC was mainly through electrostatic interactions, pore adsorption, π–π interactions, and framework coordination of ZIF-67 surface cations with TC.

Keywords: metal–organic framework; ZIF-67; tetracycline; adsorption mechanism

1. Introduction

Today, the world is facing a growing crisis in water pollution. Among the various pollutants in the water environment, antibiotics are considered to be new and persistent pollutants. Among all antibiotics, tetracycline (TC) ranks as the second most produced and utilized antibiotic in the world, with a persistent source of emissions and potential toxicity. Antibiotics have been widely used in recent years, mainly for the treatment of diseases and the promotion of animal growth, and they have antimicrobial activity against a broad spectrum of pathogenic bacteria [1,2]. The improper use of TCs not only increases possible risks to the ecosystem and human health but also leads to an increase in microbial resistance [3,4]. The inability of humans and animals to adequately absorb and metabolize drugs leads to the release of large quantities of drugs into the water in the form of their original metabolites or in their original form through urine and feces [5,6]. Antibiotics can exist in the environment for prolonged periods, leading to an abundance of drug-resistant flora and the emergence of drug-resistant genes, profoundly impacting the environment and necessitating antibiotic removal [7]. Unfortunately, conventional wastewater treatment plants are not effective in reducing the concentration of drugs [8]. Photocatalysis [9], electrochemical oxidation [10], deep oxidation [11], coagulation [12], and adsorption [13] have been commonly employed to eliminate TC from water over the past years. Adsorption treatment is considered to be one of the most promising methods due to its cost-effectiveness, operational simplicity, and environmental compatibility [14,15].

Metal–organic frameworks (MOFs) represent a novel category of porous materials comprising inorganic metal nodes and organic linkers [16], offering significant advantages

such as well-defined and adjustable structures, large specific surface area (SSA), and high porosity with ligand-unsaturated sites, thus holding considerable promise across various applications, including catalysis [17], gas adsorption [18], and separations [19].The pore size of MOFs also has a persistent, functional, and flexible structure, giving them excellent qualities for adsorption-related applications [20].

Zeolite imidazolate skeletons (ZIFs) constitute a distinct subtype of highly porous MOFs characterized by zeolite-like topology and imidazole or its derivative ligands. ZIFs are facile to synthesize, possess a large SSA, and exhibit regular pore structures. Typically, ZIF-67 is synthesized in high-temperature organic solvents, although some reports suggest that it can also be synthesized in aqueous solutions [21,22]. The synthesis of cobalt-based ZIF-67, featuring the combined stability of inorganic zeolites and the general advantages of MOFs, utilizing Co^{2+} as the central metal, has garnered significant attention [23]. The size and morphology of ZIF-67 can be readily tailored by adjusting synthesis conditions [24], offering enhanced flexibility and control for potential applications in porous materials. The studies reported on ZIF-67 used Co $(NO_3)_2 \cdot 6H_2O$ and 2-methylimidazole to prepare ZIF-67 by the vacuum high-temperature method [25,26]. However, Co $(NO_3)_2 \cdot 6H_2O$ is a hazardous chemical because of its oxidizing properties, which can cause combustion or explosion by rubbing or impacting organic materials. In contrast, $CoCl_2 \cdot 6H_2O$ has no special combustion and explosion characteristics and is safer and more reliable.

In this paper, we chose to use a simple room-temperature synthesis method to synthesize ZIF-67 as an adsorbent material for removing TC from water. The successful synthesis of ZIF-67 was verified by both physical and chemical analyses as well as detailed characterization. The related adsorption mechanism was elucidated via zeta potential analysis, identification of key functional groups involved in the adsorption process, and kinetic and thermodynamic analyses of the ZIF-67 adsorption process. The investigation of the ZIF-67 metal–organic skeleton as an adsorbent offers a theoretical foundation and novel avenue for the establishment of energy-efficient adsorbent materials.

2. Materials and Methods

2.1. Experimental Materials and Instruments

Aqueous cobalt chloride ($CoCl_2 \cdot 6H_2O$), 2-methylimidazole ($C_4H_6N_2$), and methanol (CH_3OH) were analytically pure. The magnetic stirrer (SN-MS-HZ80D) was obtained from Shanghai Shangpu Instrument Co., Ltd.(Shanghai, China), the pH meter (PHS-2F) was obtained from Shanghai Yidian Scientific Instrument Co., Ltd. (Shanghai, China), the electric constant temperature blast drying oven (DHG-9240A) was obtained from Shanghai Jinghong Equipment Co., Ltd. (Shanghai, China), the water bath constant temperature oscillator (SHZ-B) was obtained from Changzhou Nuoji Instrument Co., Ltd. (Changzhou, Jiangsu Province, China), and the double-beam UV spectrophotometer (UER-2209008) was obtained from Shanghai Meipuda Instrument Co., Ltd. (Shanghai, China).

2.2. Synthesis of ZIF-67W

ZIF-67 was prepared with slight modifications based on previously published relevant literature [27]. Amounts of 0.5948 g $CoCl_2 \cdot 6H_2O$ and 1.6420 g 2-methylimidazole were dissolved in 100 mL of methanol. The solution was sonicated for 10 min until fully dissolved. The reaction solution was then transferred into a beaker and stirred magnetically at 600 r/min for 8 h. After the reaction, it was left to stand for 24 h. The mixture was then centrifuged three times at 5000 r/min and washed with methanol three times. Finally, the collected purple precipitate was dried at 80 °C for 12 h. The purple ZIF-67 material was obtained.

2.3. Characterization

The synthetic materials' morphology was examined using an energy-dispersive X-ray spectroscopy (EDX) integrated with a field-emission scanning electron microscope (FE-SEM, S-4800, Shanghai, China). Surface functional groups were analyzed via Fourier-transform

infrared spectroscopy (FTIR, ThermoFisher Nicolet 6700, Waltham, MA, USA). The materials' crystalline phase and surface properties were assessed through X-ray diffraction (XRD, D/max-2550VB+/PC, Tokyo, Japan) and X-ray photoelectron spectroscopy (XPS, 250Xi, Escalab, MA, USA), respectively. The materials' SSA and pore size (PS) were examined by N_2 adsorption measurements using the Brunauer–Emmett–Teller (BET) approach (Autosorb iQ instrument, Shanghai City, China).

2.4. Adsorption Experimental Studies

2.4.1. Batch Experiments

A total of 50 mL of 50 mg·L^{-1} tetracycline was selected and added to 5 plastic vials (pH = 4.6); 10 mg of ZIF-67 was added, capped and sealed, sonicated for 30 min to mix well, and placed into a constant temperature shaker at 25 °C for 24 h with 200 RPM shaking. The pH of the solutions in the experiments was adjusted with 0.1 mol·L^{-1} HCl and NaOH, and all data points in the experiments had three parallel samples, and the adsorption process was evaluated by averaging the values. The adsorbed solution was filtered through a 0.22 μm inorganic filter membrane; the supernatant of the filtered solution was taken, and the absorbance at 365 nm was measured by UV spectrophotometer; and the concentration of tetracycline was calculated according to the standard curve equation.

2.4.2. Effect of the TC Solution pH

To optimize the adsorption conditions, the effects of pH and TC concentration on the removal of ZIF-67 were first explored. The pH of the tetracycline analog effluent solution was adjusted to 3, 5, 7, 9, and 11. An amount of 10 mg of ZIF-67 was placed in a plastic vial, and 50 mL of tetracycline solution of different pH values was added to simulate the effluent; finally, the vials were placed in a thermostatic shaker at 25 °C for 24 h with 200 RPM oscillation. After completing the reaction, the reaction solution was filtered, and the absorbance of TC at different pH levels was determined to calculate the adsorption.

2.4.3. Adsorption Isothermal Analysis

The impact of TC concentration on ZIF-67's adsorption was similar to that of the pH experiment. The optimal pH was determined, and solutions with concentrations of 30, 60, 90, 200, 300, 450, and 600 mg·L^{-1} were prepared. These solutions were then oscillated for 24 h under the same conditions as previously described. Subsequently, the absorbance was measured to calculate the adsorption amount of ZIF-67 at different concentrations.

2.4.4. Adsorption Kinetics

To investigate the effect of time and temperature on the adsorption effect of ZIF-67, similar to the above experimental steps, 50 mL of simulated effluent solution of tetracycline with the optimal concentration of tetracycline as described above was taken in a plastic vial (taking the optimal pH for the above experiments), and 10 mg of ZIF-67 was added, and oscillations were maintained at a frequency of 200 Hz under 25 °C conditions. The results are shown in the following table. Samples were taken at different time points 15, 30, 60, 120, 180, 240, 360, and 720 min, respectively, and the absorbance of the TC solution was determined after filtration. The adsorption of ZIF-67 was calculated with the corresponding kinetic and isotherm fits.2.4.5. Effect of Temperature

The same experimental conditions as described above were maintained at temperatures of 25 °C, 35 °C, and 55 °C and oscillated at 200 r/min for a certain time (optimal time point). Samples were taken at the same time point, filtered, and the absorbance was measured to calculate the amount of ZIF-67 adsorbed.

2.4.5. Statistical Analyses

Data statistics were performed using Excel software and SPSS 23.0 software, and one-way ANOVA models were utilized for data analyses. Adsorption models were fitted and visualized using OriginPro 9.1 software.

The adsorption capacity (AC) of TC was determined as follows (1):

$$q_e = \frac{(c_0 - c_e)V}{M} \tag{1}$$

where q_e—AC, mg·L^{-1};

c_0—TC content in the solution pre-adsorption, mg·L^{-1};

c_e—TC content in the solution post-adsorption, mg·L^{-1};

M—quantity of adsorbent material ZIF-67 used, g;

V—volume of added TC standard solution, L.

Pseudo-first/second-order (PFO, PSO) kinetics were employed to assess the AC of ZIF-67 on TC, as represented by Equations (2) and (3);

$$\text{PFO}: \ Q_t = Q_e\left(1 - e^{-k_1 t}\right) \tag{2}$$

$$\text{PSO}: Q_t = \frac{Q_e^2 k_2 t}{1 + Q_e k_2 t} \tag{3}$$

Q_t, Q_e denote the quantity of ZIF-67 adsorbed at time t and equilibrium (mg·g^{-1}); t denotes the adsorption time (min); k_1, k_2 denote the adsorption rate constants for the PFO and PSO models.

The isotherm data of ZIF-67 adsorbed TC were fitted using Freundlich and Langmuir models with fitting Equations (4) and (5);

$$\text{Freundlich model}: \ Q_e = \frac{Q_m b C_e}{1 + b C_e} \tag{4}$$

$$\text{Langmuir model}: \ Q_e = K_f C_e^n \tag{5}$$

where Q_e denotes the equilibrium AC of TC (mg·g^{-1}); C_e denotes the equilibrium content of TC.

3. Results and Discussion

3.1. Morphology of the Material

A simple and low-cost method was used to synthesize ZIF-67, as can be seen from the SEM images of ZIF-67 in Figure 1a,b; the typical rhombic dodecahedral structure and rhombohedral cubic crystals of ZIF-67 were successfully synthesized, which was confirmed from the literature [22].The SEM images show that the size of individual ZIF-67 prepared with uniform morphology and the surface of each rhombus is smooth and highly symmetric, indicating that the synthesized ZIF-67 has high purity and good crystallinity. Figure S1a–f demonstrates the Mapping and EDS plots of ZIF-67, from which it can be seen that four elements, C, O, Cl, and Co, were detected in the synthesized ZIF materials, confirming the successful synthesis of ZIF-67 materials.
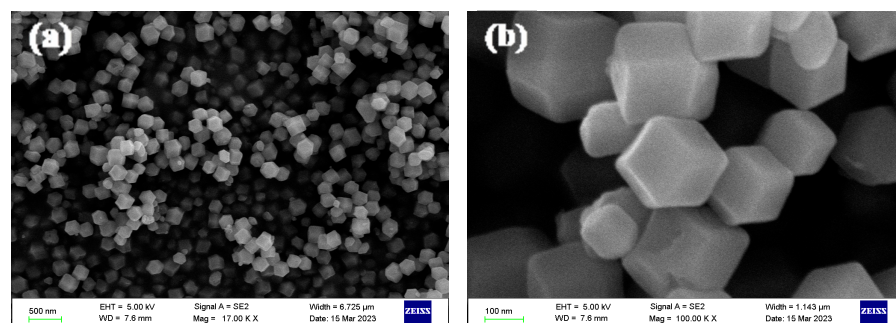

Figure 1. (**a**,**b**) SEM images of ZIF-67.

3.2. Chemical Analyses

3.2.1. FTIR Spectroscopy and XRD Assessment

Figure 2a displays the FTIR spectrum of the material. The peak at 3132.23 cm^{-1} corresponds to the generation of the N-H stretching vibration of the imidazole ring; at 2929.32 cm^{-1}, it is attributed to -CH stretching, and at 1581.32 cm^{-1} is due to C=C stretching. Those at 1141.72 cm^{-1} and 994.41 cm^{-1} are ascribed to C-O stretching, and those at 755.76 cm^{-1} and 693.90 cm^{-1} correspond to N-H stretching. The FTIR map of ZIF-67 showed that the synthesized ZIF-67 map was in agreement with previous literature reports [28]. Figure 2b shows the XRD patterns of experimental ZIF-67 for the analysis of the crystallinity of the sample. Notably, the characteristic diffraction peaks of the crystal of ZIF-67 are mainly at 7.34, 10.63, 12.72, 14.40, and 16.45, and the diffraction peaks of the above materials align with previous literature [29,30].
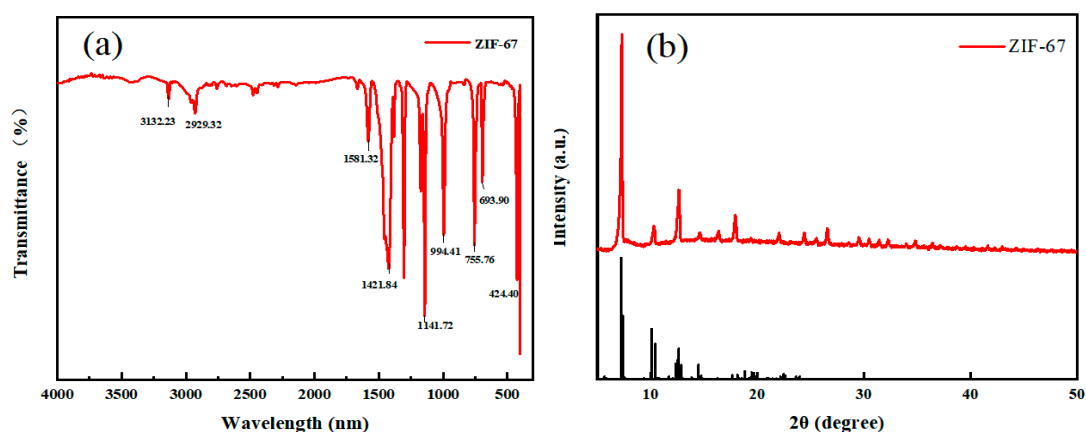

Figure 2. ZIF-67 infrared spectra (**a**), ZIF-67 X-ray diffraction (XRD) map (**b**).

3.2.2. SSA and PS Analysis

The adsorption efficiency of an adsorbent is usually related to its structural properties. The larger the PS and SSA, the higher the AC of the material [31], and the SSA is an important parameter for the study of pollutant interaction with the material surface. We cited relevant literature from Prof. Yuanyuan Li's group and found that they prepared ZIF-67 from CoCl$_2$·6H$_2$O by vacuum and high temperature. Table 1 lists the BET data of ZIF-67 prepared using the improved method, which exhibits a larger SSA and porous structure compared to the ZIF-67 prepared in the previous article.

Table 1. BET data for ZIF-67 materials.

Materials	Specific Surface Area (m^2·g^{-1})	Pore Volume (cm^3·g^{-1})	Average Pore Size (nm)	Literature Citation
ZIF-67	1245.00	0.66	/	[28]
ZIF-67	1477.00	0.71	/	[32]
ZIF-67	1334.34	0.67	1.58	[33]
ZIF-67	1463.00	0.04	/	[34]
ZIF-67	1805.97 ± 15.12	0.77 ± 0.08	2.18 ± 0.15 nm	This text

3.3. Study of TC Adsorption Properties

3.3.1. Influence of pH on the AC of ZIF-67

The AC of TC by ZIF-67 is influenced by the pH of the aqueous solution in two main aspects: TC morphology and ZIF-67 surface charge. Consequently, pH is recognized as a pivotal factor affecting the adsorption efficiency of the adsorbent. In this investigation, the impact of various pH values (range: 3–11) on TC adsorption was explored, and the experimental findings are demonstrated in Figure 3a.
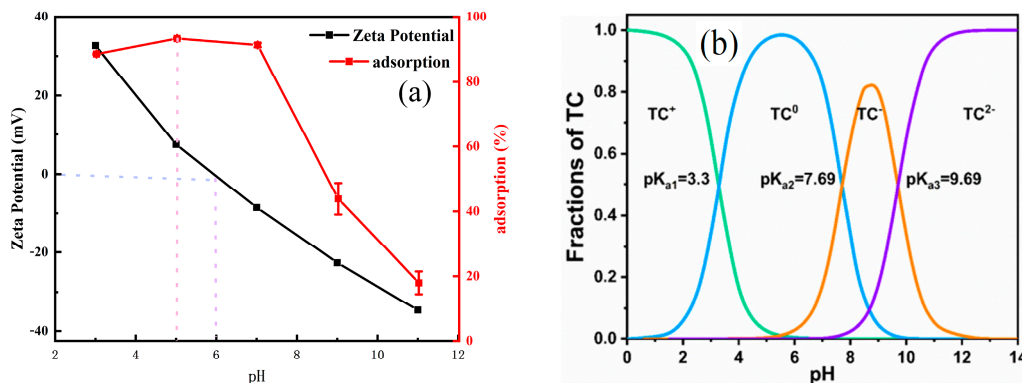
Figure 3. (**a**) represents the adsorption of TC by ZIF-67 at different pH values and the zeta potential of ZIF-67 at different pH values, and (**b**) represents the morphological distribution of TC at different pH values.

TC exists in different forms at different pH conditions, as cationic, anionic, and amphoteric ions, respectively [35]. As shown in Figure 3b, TC occurs mainly in the cationic state (TCH_3^+) when pH < 3.3. When 3.3 < pH < 7.7, TC converts to amphoteric species (TCH_2^0) and anionic species (TCH^-). When pH > 7.7, it converts to anionic species (TC^{2-}) [36].

As displayed in Figure 3a, the pH significantly influences the AC of TC by ZIF-67 material. The adsorption rate of TC increases initially and then decreases as the pH varies within the range of pH = 3.0–11.0. As depicted in the figure, the adsorption rate of ZIF-67 on TC gradually rises as the pH increases from 3 to 5. For some organic pollutants, the main factors affecting the adsorption process include the pollutant's state of existence and the charge on the adsorbent's surface. Therefore, ZIF-67 was subjected to zeta potential measurements, revealing a positively charged surface in the pH = 3–6 range (see Figure 3a). As the pH gradually increases, the morphology of TC changes to TCH^{3+}-TCH_2^0-TCH^{-1}. The adsorption rate shows a trend of first increasing and then decreasing with the increase of pH and reaches its highest value at pH = 5. When the pH is around 5, positively charged materials adsorb TC, which may be due to electrostatic interactions. At the same time, as the pH gradually rises, the concentration of H^+ decreases, leading to the degradation of numerous functional groups on the ZIF-67 surface. Consequently, TCH_2^0 gains more available adsorption sites [37]. However, the adsorption of TC by ZIF-67 gradually diminishes as the pH increases from 6 to 11. Given the negatively charged surface of ZIF-67 and the predominant existence of TC in the forms of TCH^{-1} and TC^{2-}, the reduction in adsorption by ZIF-67 primarily stems from electrostatic repulsion between them, resulting in a notable reduction in the adsorption rate.

3.3.2. Study of the Impacts of Contact Time and Adsorption Kinetics

Adsorption kinetics elucidates the relationships between adsorption duration and the amount of adsorption. Figure 4a demonstrates the impact of time on the AC of ZIF-67 on TC. The findings reveal a gradual increase in the adsorption of ZIF-67 on TC with extended time. Notably, the adsorption rate escalates rapidly as the duration extends from 30 min to 450 min. Subsequently, the adsorption gradually stabilizes as the duration progresses from 450 min to 720 min, resulting in maximum equilibrium adsorption at 720 min. To clarify the adsorption mechanisms of ZIF-67 on TC, PFO, PSO, and Elovich models were analyzed (Figure 4). Table 2 lists the parameters of the PFO and PSO models, as well as the Elovich model for fitting ZIF-67 adsorption of TC. Notably, the PFO model fails to describe the experimental data adequately, with a low correlation coefficient ($R^2 = 0.78341$) and small q_e values. In contrast, the PSO kinetic model exhibits a superior correlation coefficient ($R^2 = 0.968$) compared to the pseudo-first-order model, suggesting its applicability in describing the adsorption behaviors of ZIF-67 on TC. Moreover, the

pseudo-secondary kinetic q_e of 1533.47 correlates well with experimentally measured q_e, implying chemisorption predominates the adsorption process [38,39]. Furthermore, the adsorption kinetic data of ZIF-67 on TC align well with the Elovich model ($R^2 > 0.954$), suggesting a non-homogeneous phase diffusion process according to the fitting results of the intra-particle diffusion model, Figure S3. Intriguingly, intra-particle diffusion modeling reveals two stages of adsorption, namely intra-particle diffusion modeling and surface binding. Additionally, the slightly deviated fitted curves from the origin indicate that intra-particle diffusion modeling is merely one of the factors influencing the absorption rate [40]. This underscores the likelihood of other factors influencing the adsorption performance of TC by ZIF-67. Moreover, the fitting results are corroborated with multivariate linear correlations, underscoring that ZIF-67 adsorption of TC involves multiple mechanisms, potentially influenced by a combination of factors.
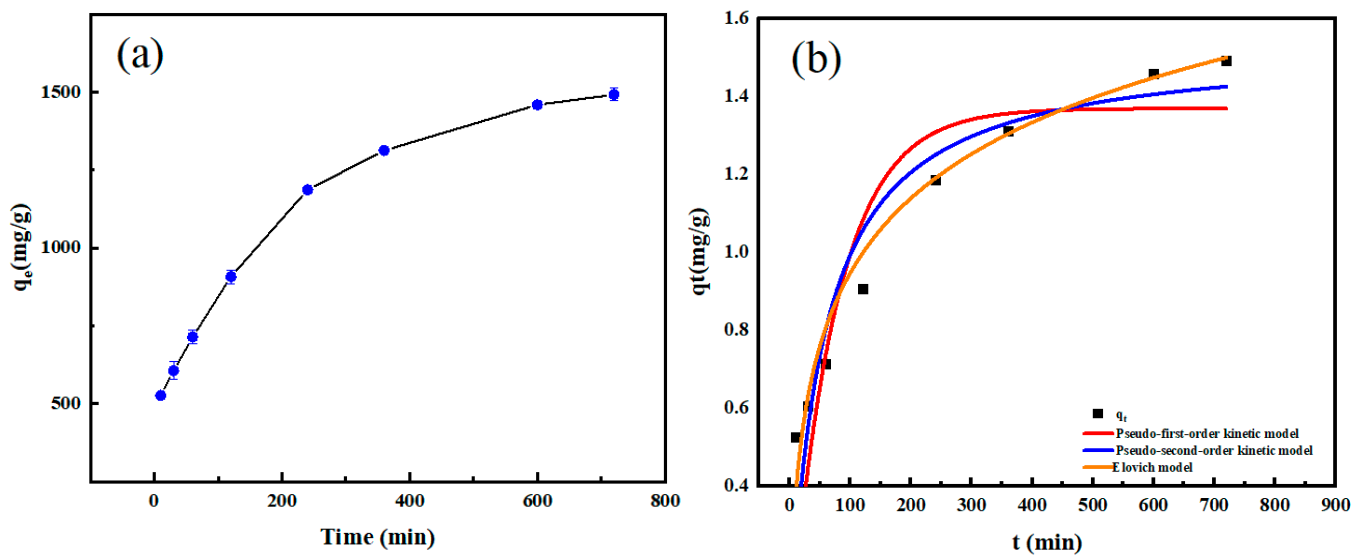

Figure 4. Effect of time on TC adsorption by ZIF-67 (**a**), pseudo-primary kinetics, pseudo-secondary kinetics, Elovich model for TC adsorption by ZIF-67 at different times (**b**) (Inset: Intra-particle diffusion model).

Table 2. Fitting parameters of the kinetic model for TC adsorption by ZIF-67.

Material	Pseudo-First-Order Kinetic Model			Pseudo-Second-Order Kinetic Model			Elovich Model		
	k_1 (min^{-1})	q_e (mg·g^{-1})	R^2	k_2 (min^{-1})	q_e (mg·g^{-1})	R^2	a (mg·g^{-1})	b (g·mg^{-1}·h^{-1})	R^2
ZIF-67	0.013	1369.738	0.783	1.200	1533.470	0.968	100.200	0.038	0.954

3.3.3. Impact of Initial Content and Study of Adsorption Isotherms

The impact of initial TC content on the AC of ZIF-67 is shown in Figure 5, revealing a rapid increase in adsorption as the content increases from 30 mg·L^{-1} to 300 mg·L^{-1}. However, beyond 300 mg·L^{-1}, the rate of adsorption increases gradually, ultimately reaching equilibrium at 600 mg·L^{-1}. This suggests that a higher initial concentration facilitates the adsorption process. Considering the prolonged dissolution time required for a concentration of 600 mg·L^{-1}, 450 mg·L^{-1} was selected as the optimal concentration. To further understand the interactions among ZIF-67 material and TC, the experimental adsorption isotherm data were fitted by Langmuir, Freundlich, and Temkin isothermal adsorption models. As presented in Table 3, the Langmuir model exhibits a maximum correlation coefficient ($R^2 = 0.976$) compared to Freundlich and Temkin, indicating its suitability in describing the adsorption of ZIF-67 on TC, primarily as a monolayer adsorption behavior [41].The Freundlich model also had a high fit with an R coefficient of 0.945, and both the Langmuir

model and the Freundlich model could adequately express the adsorption performance of ZIF-67 on TC. This result suggests that TC adsorption by ZIF-67 is a coexistence of monolayer and multilayer adsorption, with monolayer adsorption as the main adsorption process [42,43]. The calculated adsorption q_m based on Langmuir's equation is 1707.666, which closely aligns with experimental findings, suggesting uniform TC coverage on ZIF-67.
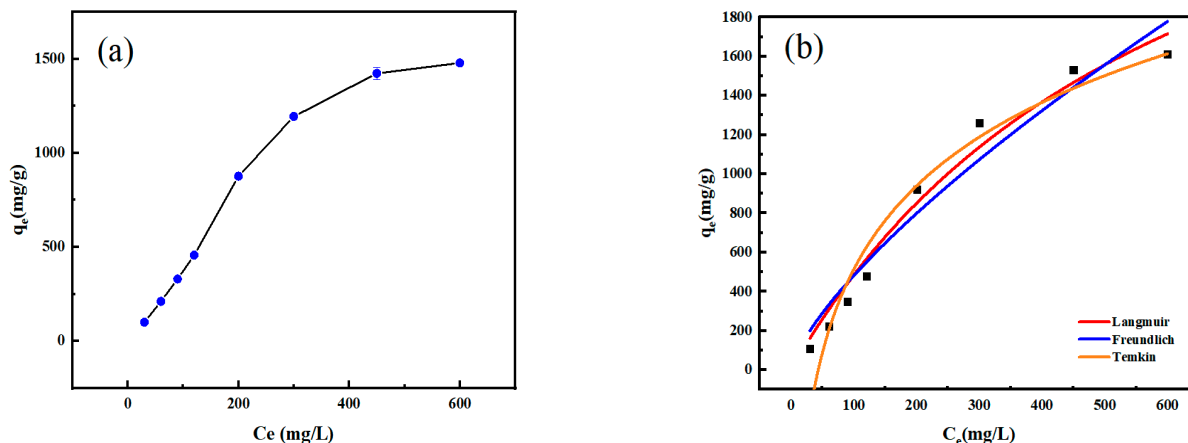

Figure 5. Effect of initial concentration on TC adsorption by ZIF-67 (**a**), isotherm of TC adsorption by ZIF-67 (**b**).

Table 3. Fitting parameters of ZIF-67 adsorption TC isothermal model.

Material	Langmuir			Freundlich			Temkin		
	q_m (mg·g^{-1})	K_L (L·mg^{-1})	R^2	K_F (mg^{1-n}·g^{-1}·L^n)	n	R^2	a	b	R^2
ZIF-67	1707.666	0.002	0.976	16.841	1.372	0.945	0.023	0.598	0.936

3.3.4. Effect of Temperature on TC Adsorption Properties

Temperature plays a vital role in the adsorption process, and Figure 6 demonstrates the amount of TC adsorbed by ZIF-67 at 298, 308, and 328 K. Notably, the adsorption of ZIF-67 on TC increases with increasing temperature. The relationships among ln(K) and 1/T were fitted, and the findings are displayed in Figure S2. ΔH and ΔS can be computed from the slopes and intercepts of the straight lines, and the associated thermodynamic parameters are shown in Table S1. When ΔH > 0, it indicates that the adsorption of ZIF-67 on TC is a heat-absorbing process, demonstrating an increased interest in adsorption at elevated temperatures [44]. Furthermore, ΔG < 0 signifies that the adsorption process is spontaneous at the time of adsorption [45]. Additionally, ΔS > 0 indicates an increased randomness in the adsorption process [46].

Table 4 compares the adsorption performance of different adsorbents under optimal conditions for TC. The results indicate that, in comparison to other adsorbent materials, ZIF-67 exhibits a particularly high adsorption capacity for TC.

Table 4. Comparison of the adsorption capacity of various adsorbents for TC.

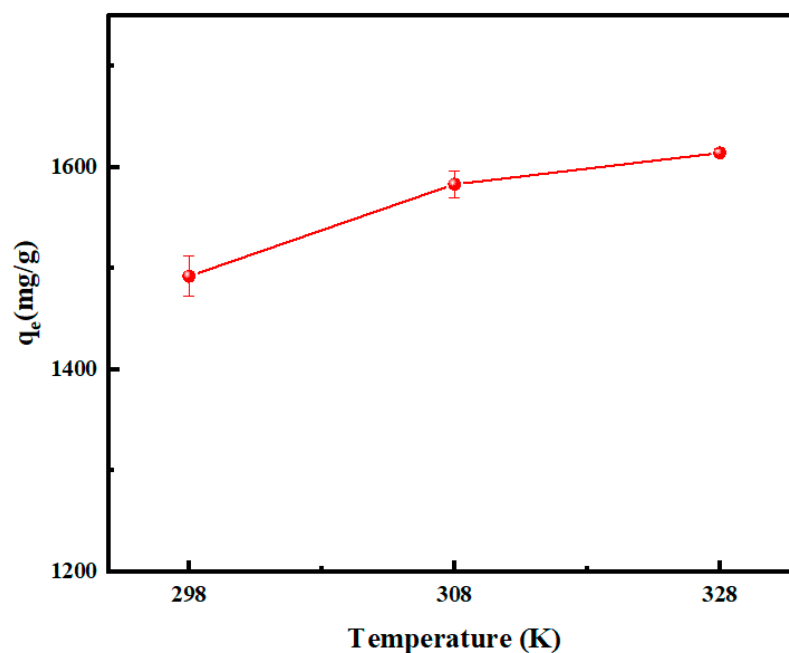| Adsorbent	pH Value	q_{max} (mg·g^{-1})	References
Carbon-doped boron nitride (BCN)	7.8	76.74	[36]
ZnO-NP@Zn-MOF-74	5.5	137.17	[47]
MOF-525/GO	3	436	[48]
P-MIL-100	8	826.45	[49]
ZIF-MIL-4	2	1288	[50]
ZIF-67	5	1583.13	This work

Figure 6. Adsorption of ZIF-67 on TC at different temperatures.

3.4. Mechanism Analysis

3.4.1. SEM Analysis

Figure 7a–c shows the SEM images of ZIF-67 after adsorption of TC, which undergoes agglomeration after adsorption of TC and becomes rougher but still maintains its original angularity. It indicates that the surface of the material was slightly modified after ZIF-67 adsorbed on TC, and there was no significant change in the morphology and crystal form.
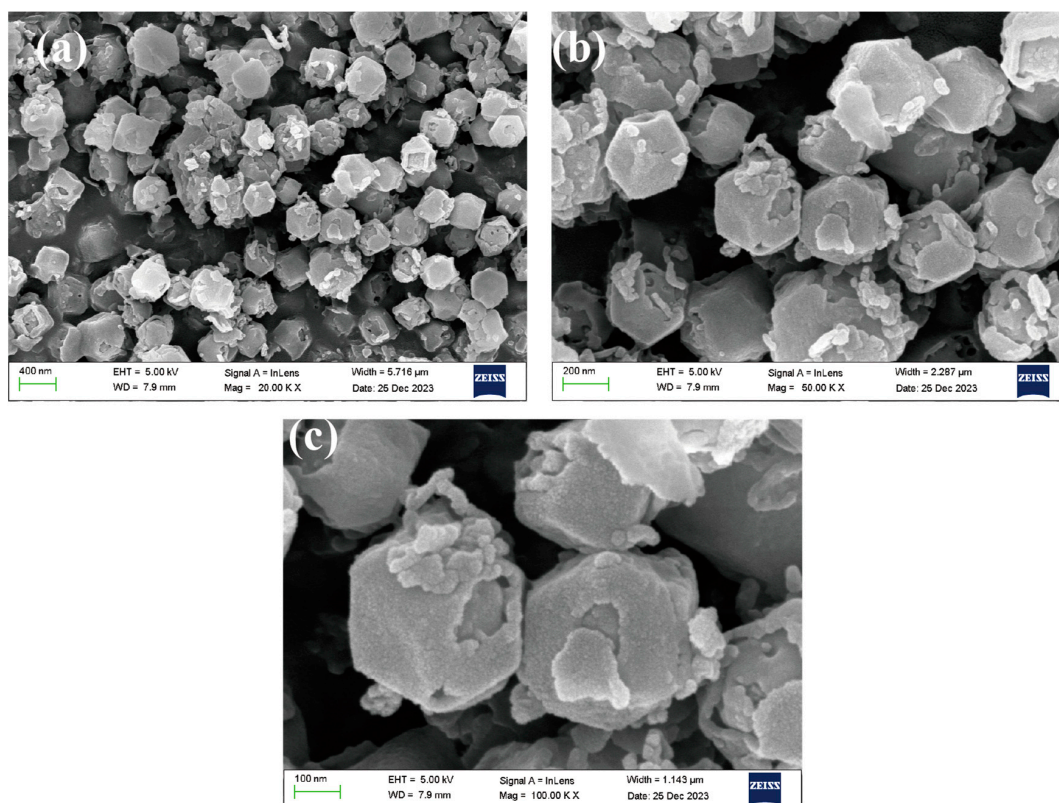

Figure 7. (**a**–**c**) represent SEM images of ZIF-67 after adsorption of TC, respectively.

3.4.2. Infrared Spectra of ZIF-67

To elucidate the mechanism of TC adsorption in water by ZIF-67, the FTIR maps of ZIF-67 before and after the reaction were analyzed for the study of the sample's surface functional groups. Figure 8 shows the FTIR comparison of ZIF-67 pre- and post-adsorption of TC. The main changes occurred in the adsorption intensity of each peak, suggesting that the backbone structure of ZIF-67 is still stable after absorbing TC [51]. The broad peak of ZIF-67 at 3408.96 cm^{-1} after adsorption of TC is attributed to the presence of -OH, possibly due to residual moisture in the material. The peak at 1581 cm^{-1} after adsorption was obscured by a strong peak appearing at 1596 cm^{-1}, indicating the presence of a benzene ring [52]. TC was adsorbed onto ZIF-67 due to its abundant conjugated benzene ring structure and multiple phenolic hydroxyl groups [53], further confirming that the adsorption occurs through π–π interactions and cation–π bonds [54]. In addition, the bending vibrational peaks of C-H at 1380.85 cm^{-1}, C-N at 1303.86 cm^{-1}, C-O at 1141.72 cm^{-1}, and N-H at 755.76 cm^{-1} were significantly weakened, as well as the stretching vibrational peak of Co-N at 424.40 cm^{-1} [55], which further suggests potential interactions among ZIF-67 and TC.
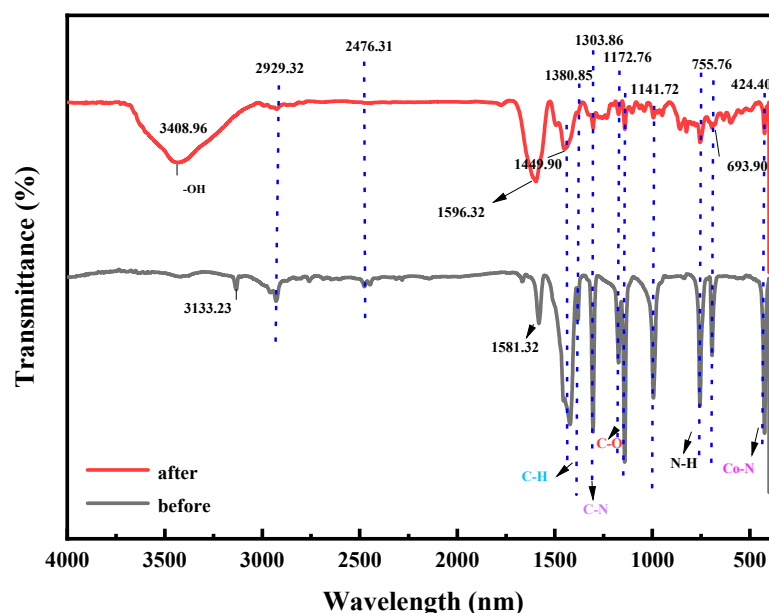

Figure 8. FTIR plots of ZIF-67 before and after TC adsorption.

3.4.3. XPS Infrared Spectrograms

The XPS spectral data of ZIF-67 pre- and post-adsorption of TC are shown in Figure 9, where XPS was employed to validate the oxidation state and chemical composition of ZIF-67 before and after adsorption. The measured spectrogram in Figure 9a shows that ZIF-67 consists of the elements Co, C, N, O, and Cl [56], and the adsorption of TC results in a slight shift of the Co 2p peak, which occurs due to the interaction of ZIF-67 with TC. The detailed spectral analysis of ZIF-67 is shown in Figure 9c,d, while Figure 9b displays two peaks of C 1S at 284.83 (eV), 285.35 (eV), corresponding to C=C and C=N bonds, respectively. The peak of C=O bonding at 288.60 (eV) after adsorption confirms its significant role in TC adsorption by ZIF-67. Figure 9c shows the O 1s spectra of oxygen pre- and post-adsorption of TC, showing a -OH peak at 531.59 and a peak at 533.04 (eV) corresponding to C=O. After adsorption of TC by ZIF-67, the intensity of the -OH peak at 531.59 decreased, indicating that -OH plays an essential role in the adsorption process, while the peak at 532.33 (eV) changed at a larger magnitude, indicating the substantial involvement of C=O in the adsorption process. Figure 9d shows the Co 2p spectrum with two peaks observed at 782.72 eV and 804.64 eV, attributed to Co 2p3/2 and Co 2p1/2 of Co^{2+}, respectively [56]. The Co 2p spectra after adsorption of TC showed a substantial

reduction of the wave peaks compared to the pure ZIF-67 spectrograms, suggesting a lower content of elemental Co, further confirming the interaction between ZIF-67 and TC.
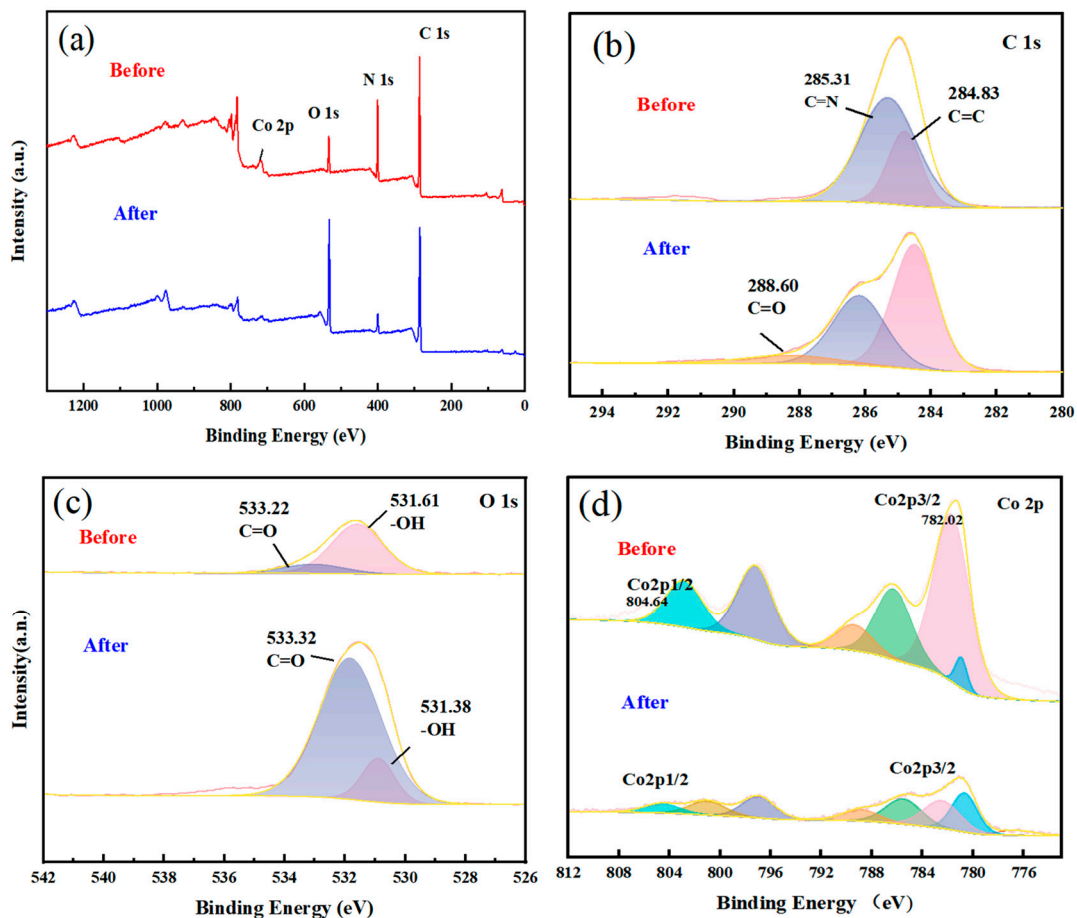

Figure 9. (**a**–**d**) represent the XPS images of ZIF-67 before and after TC adsorption, respectively.

3.4.4. Pore Size Adsorption

ZIF-67 has a large SSA and PS, both of which may influence adsorption. According to previous literature reports [57], the molecular volume of TC is 0.43, much smaller than the PS of ZIF-67. An appropriate PS can promote the pollutants to enter into the adsorbent's pores, granting access to active sites and enhancing adsorption efficacy [57].

3.5. Evaluation of Cycling Performance

The cycling performance of the recovered ZIF-67 was analyzed, and it can be seen from Figure 10a that after three consecutive cycles, the adsorption of TC by ZIF-67 retained 55.65% of its initial AC. The slight decrease in the removal rate might be attributed to incomplete resolution during the elution process. In Figure 10b, the XRD analysis of the regenerated composite illustrates that after the first reuse, the diffraction peaks corresponding to ZIF-67 remained unchanged, and the peaks were significantly weakened. This implies that the crystalline structures of ZIF-67 remain intact after one recycling, affirming its reusability.
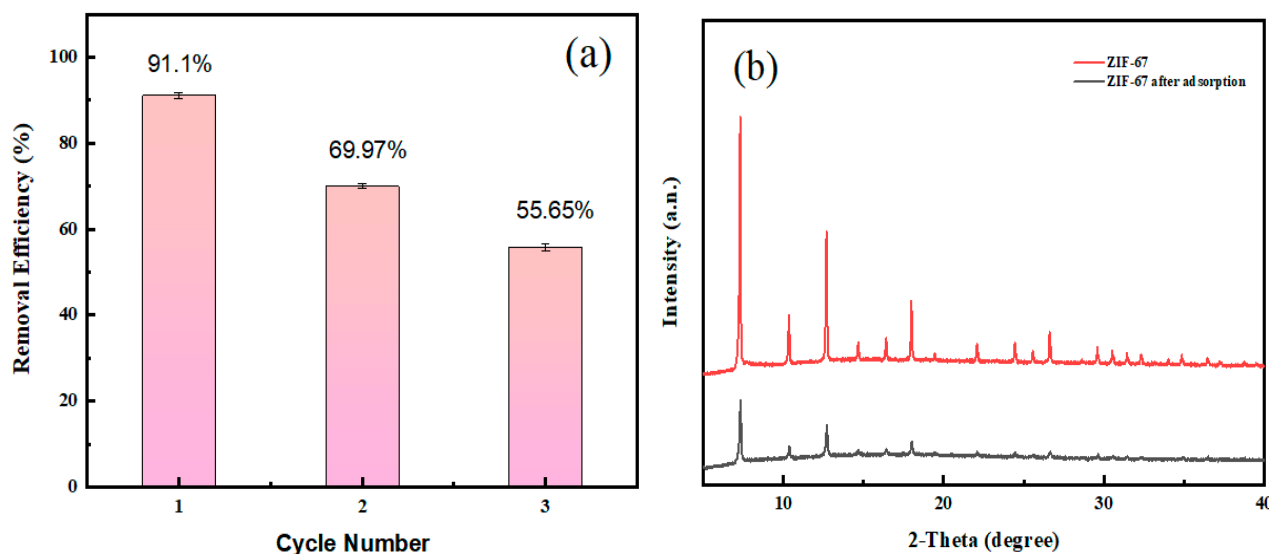
Figure 10. (**a**) Recycling of ZIF-67, (**b**) XRD plots before and after recycling of ZIF-67.

4. Conclusions

In summary, ZIF-67 micro- and nanoparticles with a high SSA and porous structure were synthesized through a simple method at room temperature. The successful synthesis of ZIF-67 was confirmed by SEM-EDS, FTIR, XRD, XPS, and other characterization methods. The impacts of parameters, including solution pH, initial TC content, reaction temperature, and time of TC removal, were investigated by batch experiments. The findings demonstrated that the adsorption and removal effect of ZIF-67 on TC could reach up to 1583.128 mg·L^{-1}. Kinetic and thermodynamic analyses revealed that the adsorption of TC by ZIF-67 followed a second-order reaction and adhered to the Langmuir model, suggesting that TC adsorption was primarily governed by chemisorption and monolayer adsorption mechanisms. Mechanistic studies further indicated that the adsorption process is a major role of C=O functional groups and π–π bonds on the TC surface. Repeated experiments showed that the structure of ZIF-67 could remain unchanged after washing and drying after adsorption of TC, and ZIF-67 could be a promising adsorbent material.

absence of any commercial or financial relationships that could be construed as a potential conflict of interest.

References

1. Nguyen, V.-T.; Nguyen, T.-B.; Chen, C.-W.; Hung, C.-M.; Hien Vo, T.-D.; Chang, J.-H.; Dong, C.-D. Influence of pyrolysis temperature on polycyclic aromatic hydrocarbons production and tetracycline adsorption behavior of biochar derived from spent coffee ground. *Bioresour. Technol.* **2019**, *284*, 197–203. [CrossRef]
2. Polubesova, T.; Zadaka, D.; Groisman, L.; Nir, L. Water remediation by micelle–clay system: Case study for tetracycline and sulfonamide antibiotics. *Water Res.* **2006**, *40*, 2369–2374. [CrossRef]
3. Cao, J.; Lai, L.; Lai, B.; Yao, G.; Chen, X.; Song, L. Degradation of tetracycline by peroxymonosulfate activated with zero-valent iron: Performance, intermediates, toxicity and mechanism. *Chem. Eng. J.* **2019**, *364*, 45–56. [CrossRef]
4. Chen, J.; Gao, Q.; Zhang, X.; Liu, Y.; Wang, P.; Jiao, Y.; Yang, Y. Nanometer mixed-valence silver oxide enhancing adsorption of ZIF-8 for removal of iodide in solution. *Sci. Total Environ.* **2019**, *646*, 634–644. [CrossRef] [PubMed]
5. Zhu, X.; Liu, Y.; Zhou, C.; Luo, G.; Zhang, S.; Chen, J. A novel porous carbon derived from hydrothermal carbon for efficient adsorption of tetracycline. *Carbon* **2014**, *77*, 627–636. [CrossRef]
6. Wang, C.; Lin, C.-Y.; Liao, G.-Y. Degradation of antibiotic tetracycline by ultrafine-bubble ozonation process. *J. Water Process Eng.* **2020**, *37*, 101463. [CrossRef]
7. Pulicharla, K.H.R.; Brar, S.K.; Surampalli, R.Y. Tetracyclines metal complexation: Significance and fate of mutual existence in the environment. *Environ. Pollut.* **2017**, *221*, 1–14. [CrossRef] [PubMed]
8. Shamsudin, M.S.; Azha, S.F.; Sellaoui, L.; Badawi, M.; Al-Ghamdi, Y.; Petriciolet, A.B.; Ismail, S. Fabrication and characterization of a thin coated adsorbent for antibiotic and analgesic adsorption: Experimental investigation and statistical physical modelling. *Chem. Eng. J.* **2020**, *401*, 126007. [CrossRef]
9. Luo, J.; Ning, X.; Zhan, L.; Zhou, X. Facile construction of a fascinating Z-scheme AgI/Zn$_3$V$_2$O$_8$ photocatalyst for the photocatalytic degradation of tetracycline under visible light irradiation. *Sep. Purif. Technol.* **2021**, *255*, 117691. [CrossRef]
10. Xu, S.; Lv, Y.; Zhang, Y. 3D hydrangea-like Mn$_3$O$_4$@(PSS/PDDA/Pt)n with ultrafine Pt nanoparticles modified anode for electrochemical oxidation of tetracycline. *J. Taiwan Inst. Chem. Eng.* **2020**, *112*, 240–250. [CrossRef]
11. Xing, H.; Gao, S.; Zhang, J.; Xu, Y.; Du, H.; Zhu, Z.; Wang, J.; Yao, Y.; Zhang, S.; Ren, L. Ultrasound-assisted synthesized BiFeO$_3$ as FeOH+ promoted peroxymonosulfate activator for highly efficient degradation of tetracycline. *J. Alloys Compd.* **2021**, *854*, 157281. [CrossRef]
12. Saitoh, T.; Shibata, K.; Fujimori, K.; Ohtani, Y. Rapid removal of tetracycline antibiotics from water by coagulation-flotation of sodium dodecyl sulfate and poly(allylamine hydrochloride) in the presence of Al(III) ions. *Sep. Purif. Technol.* **2017**, *187*, 76–83. [CrossRef]
13. Wang, J.; Lei, S.; Liang, L. Preparation of porous activated carbon from semi-coke by high temperature activation with KOH for the high-efficiency adsorption of aqueous tetracycline. *Appl. Surf. Sci.* **2020**, *530*, 147187. [CrossRef]
14. Gao, Y.; Liu, K.; Kang, R.; Xia, J.; Yu, G.; Deng, S. A comparative study of rigid and flexible MOFs for the adsorption of pharmaceuticals: Kinetics, isotherms and mechanisms. *J. Hazard. Mater.* **2018**, *359*, 248–257. [CrossRef] [PubMed]
15. Jiang, J.; Zhang, X.; Zhu, X.; Li, Y. Removal of Intermediate Aromatic Halogenated DBPs by Activated Carbon Adsorption: A New Approach to Controlling Halogenated DBPs in Chlorinated Drinking Water. *Environ. Sci. Technol.* **2017**, *51*, 3435–3444. [CrossRef] [PubMed]
16. Furukawa, H.; Cordova, K.E.; O'Keeffe, M.; Yaghi, O.M. The Chemistry and Applications of Metal-Organic Frameworks. *Science* **2013**, *341*, 1230444. [CrossRef]
17. Si, Y.; Li, Y.; Zou, J.; Xiong, X.; Zeng, X.; Zhou, J. Photocatalytic Performance of a Novel MOF/BiFeO$_3$ Composite. *Materials* **2017**, *10*, 1161. [CrossRef]
18. Challagulla, S.; Payra, S.; Rameshan, R.; Roy, S. Low temperature catalytic reduction of NO over porous Pt/ZIF-8. *J. Environ. Chem. Eng.* **2020**, *8*, 103815. [CrossRef]
19. Liu, X.; Wang, M.; Zhou, S.; Wang, J.; Xin, H.; Wei, S.; Liu, S.; Wang, Z.; Lu, X. Tracking CO$_2$ capture and separation over N$_2$ in a flexible metal–organic framework: Insights from GCMC and DFT simulations. *J. Mater. Sci.* **2021**, *56*, 10414–10423. [CrossRef]
20. Cychosz, K.A.; Wong-Foy, A.G.; Matzger, A.J. Liquid Phase Adsorption by Microporous Coordination Polymers: Removal of Organosulfur Compounds. *J. Am. Chem. Soc.* **2008**, *130*, 6938–6939. [CrossRef]
21. Feng, X.; Wu, T.; Carreon, M.A. Synthesis of ZIF-67 and ZIF-8 crystals using DMSO (Dimethyl Sulfoxide) as solvent and kinetic transformation studies. *J. Cryst. Growth* **2016**, *455*, 152–156. [CrossRef]
22. Qian, J.; Sun, F.; Qin, L. Hydrothermal synthesis of zeolitic imidazolate framework-67 (ZIF-67) nanocrystals. *Mater. Lett.* **2012**, *82*, 220–223. [CrossRef]
23. Dong, Y.; Zheng, J. Environmentally friendly synthesis of Co-based zeolitic imidazolate framework and its application as H$_2$O$_2$ sensor. *Chem. Eng. J.* **2020**, *392*, 123690. [CrossRef]
24. Hu, Y.; Li, W.; Wei, Z.; Yang, H.; Li, S. Advances in electrochemical sensing with ZIF-67 and related materials. *Int. J. Electrochem. Sci.* **2023**, *18*, 100180. [CrossRef]
25. Sohouli, E.; Karimi, M.S.; Khosrowshahi, E.M.; Rahimi-Nasrabadi, M.; Ahmadi, F. Fabrication of an electrochemical mesalazine sensor based on ZIF-67. *Measurement* **2020**, *165*, 108140. [CrossRef]

26. Tang, J.; Hui, Z.-Z.; Hu, T.; Cheng, X.; Guo, J.-H.; LI, Z.-R.; Yu, H. A sensitive acetaminophen sensor based on Co metal–organic framework (ZIF-67) and macroporous carbon composite. *Rare Met.* **2022**, *41*, 189–198. [CrossRef]

27. Yang, L.; Li, H.; Yu, Y.; Wu, Y.; Zhang, L. Assembled 3D MOF on 2D Nanosheets for Self-boosting Catalytic Synthesis of N-doped Carbon Nanotube Encapsulated Metallic Co Electrocatalysts for Overall Water Splitting. *Appl. Catal. B Environ.* **2020**, *271*, 118939. [CrossRef]

28. Khan, A.; Ali, M.; Ilyas, A.; Naik, P.; Vankelecom, I.F.; Gilani, M.A.; Bilad, M.R.; Sajjad, Z.; Khan, A.L. ZIF-67 filled PDMS mixed matrix membranes for recovery of ethanol via pervaporation. *Sep. Purif. Technol.* **2018**, *206*, 50–58. [CrossRef]

29. Chen, G.; He, S.; Shi, G.; Ma, Y.; Ruan, C.; Jin, X.; Chen, Q.; Liu, X.; Dai, H.; Chen, X.; et al. In-situ immobilization of ZIF-67 on wood aerogel for effective removal of tetracycline from water. *Chem. Eng. J.* **2021**, *423*, 130184. [CrossRef]

30. Xue, Y.; Xiang, P.; Wang, H.; Jiang, Y.; Long, Y.; Lian, H.; Shi, W. Mechanistic insights into selective adsorption and separation of multi-component anionic dyes using magnetic zeolite imidazolate framework-67 composites. *J. Mol. Liq.* **2019**, *296*, 111990. [CrossRef]

31. Song, M.; Wei, Y.; Yu, L.; Tang, X. The application of prepared porous carbon materials: Effect of different components on the heavy metal adsorption. *Waste Manag. Res.* **2016**, *34*, 534–541. [CrossRef]

32. Liu, Y.; Gonçalves, A.A.; Zhou, Y.; Jaroniec, M. Importance of surface modification of γ-alumina in creating its nanostructured composites with zeolitic imidazolate framework ZIF-67. *J. Colloid Interface Sci.* **2018**, *526*, 497–504. [CrossRef]

33. Yinan, W.J.L. Novel functionalization of ZIF-67 for an efficient broad-spectrum photocatalyst: Formaldehyde degradation at room temperature. *New J. Chem.* **2022**, *46*, 2962–2970.

34. Li, Y.; Jin, Z.; Zhao, T. Performance of ZIF-67—Derived fold polyhedrons for enhanced photocatalytic hydrogen evolution. *Chem. Eng. J.* **2020**, *382*, 123051. [CrossRef]

35. Qiang, Z.; Adams, C. Potentiometric determination of acid dissociation constants (pKa) for human and veterinary antibiotics. *Water Res.* **2004**, *38*, 2874–2890. [CrossRef]

36. Guo, Y.; Yan, C.; Wang, P.; Rao, L.; Wang, C. Doping of carbon into boron nitride to get the increased adsorption ability for tetracycline from water by changing the pH of solution. *Chem. Eng. J.* **2020**, *387*, 124136. [CrossRef]

37. Guixia, Z. Removal of Pb(ii) ions from aqueous solutions on few-layered graphene oxide nanosheets. *Dalton Trans.* **2011**, *40*, 10945–10952.

38. Zhong, X.; Lu, Z.; Liang, W.; Hu, B. The magnetic covalent organic framework as a platform for high-performance extraction of Cr(VI) and bisphenol a from aqueous solution. *J. Hazard. Mater.* **2020**, *393*, 122353. [CrossRef] [PubMed]

39. Yang, J.; Ma, C.; Tao, J.; Li, J.; Du, K.; Wei, Z.; Chen, C.; Wang, Z.; Zhao, C.; Ma, M. Optimization of polyvinylamine-modified nanocellulose for chlorpyrifos adsorption by central composite design. *Carbohydr. Polym.* **2020**, *245*, 116542. [CrossRef] [PubMed]

40. Qu, J.; Dong, M.; Bi, F.; Tao, Y.; Wang, L.; Jiang, Z.; Zhang, G.; Zhang, B.; Zhang, Y. Microwave-assisted one-pot synthesis of β-cyclodextrin modified biochar for stabilization of Cd and Pb in soil. *J. Clean. Prod.* **2022**, *346*, 131165. [CrossRef]

41. Liu, H.; Xu, G.; Li, G. Preparation of porous biochar based on pharmaceutical sludge activated by NaOH and its application in the adsorption of tetracycline. *J. Colloid Interface Sci.* **2021**, *587*, 271–278. [CrossRef]

42. Yin, Q.; Nie, Y.; Han, Y.; Wang, R.; Zhao, Z. Properties and the Application of Sludge-Based Biochar in the Removal of Phosphate and Methylene Blue from Water: Effects of Acid Treating. *Langmuir* **2022**, *38*, 1833–1844. [CrossRef]

43. Li, C.; Zhang, N.; Chen, J.; Ji, J.; Liu, X.; Wang, J.; Wang, J.; Zhu, J.; Ma, Y.L. Temperature and pH sensitive composite for rapid and effective removal of sulfonylurea herbicides in aqueous solution. *Environ. Pollut.* **2019**, *255*, 113150. [CrossRef]

44. Qu, J.; Wang, S.; Jin, L.; Liu, Y.; Yin, R.; Jiang, Z.; Tao, Y.; Huang, J.; Zhang, Y. Magnetic porous biochar with high specific surface area derived from microwave-assisted hydrothermal and pyrolysis treatments of water hyacinth for Cr(VI) and tetracycline adsorption from water. *Bioresour. Technol.* **2021**, *340*, 125692. [CrossRef] [PubMed]

45. Wang, W.; Gao, M.; Cao, M.; Dan, J.; Yang, H. Self-propagating synthesis of Zn-loaded biochar for tetracycline elimination. *Sci. Total Environ.* **2021**, *759*, 143542. [CrossRef] [PubMed]

46. Qu, J.; Zhang, W.; Bi, F.; Yan, S.; Miao, X.; Zhang, B.; Wang, Y.; Ge, C.; Zhang, Y. Two-step ball milling-assisted synthesis of N-doped biochar loaded with ferrous sulfide for enhanced adsorptive removal of Cr(VI) and tetracycline from water. *Environ. Pollut.* **2022**, *306*, 119398. [CrossRef]

47. Guo, Z.; Yang, F.; Yang, R.; Sun, L.; Li, Y.; Xu, J. Preparation of novel ZnO-NP@Zn-MOF-74 composites for simultaneous removal of copper and tetracycline from aqueous solution. *Sep. Purif. Technol.* **2021**, *274*, 118949. [CrossRef]

48. Chen, B.; Li, Y.; Li, M.; Cui, M.; Xu, W.; Li, L.; Sun, Y.; Wang, M.; Zhang, Y.; Chen, K. Rapid adsorption of tetracycline in aqueous solution by using MOF-525/graphene oxide composite. *Microporous Mesoporous Mater.* **2021**, *328*, 111457. [CrossRef]

49. Wu, J.; Gao, Y.; Wei, S.; Chen, P.; Gu, D.; Fu, B.; Chen, M. Plasma modification of Fe-MOF for efficient organic pollutants removal. *J. Solid State Chem.* **2021**, *302*, 122350. [CrossRef]

50. Zhong, U. High-performance and selective adsorption of ZIF-8/MIL-100 hybrids towards organic pollutants. *Nanoscale Adv.* **2022**, *4*, 1431–1444. [CrossRef] [PubMed]

51. Saghir, S.; Xiao, Z. Facile preparation of metal-organic frameworks-8 (ZIF-8) and its simultaneous adsorption of tetracycline (TC) and minocycline (MC) from aqueous solutions. *Mater. Res. Bull.* **2021**, *141*, 111372. [CrossRef]

52. Li, N.; Zhou, L.; Jin, X.; Owens, G.; Chen, Z. Simultaneous removal of tetracycline and oxytetracycline antibiotics from wastewater using a ZIF-8 metal organic-framework. *J. Hazard. Mater.* **2019**, *366*, 563–572. [CrossRef]

53. Yu, R.; Wu, Z. High adsorption for ofloxacin and reusability by the use of ZIF-8 for wastewater treatment. *Microporous Mesoporous Mater.* **2020**, *308*, 110494. [CrossRef]

54. Tian, N.; Jia, Q.; Su, H.; Zhi, Y.; Ma, A.; Wu, J.; Shan, S. The synthesis of mesostructured NH2-MIL-101(Cr) and kinetic and thermodynamic study in tetracycline aqueous solutions. *J. Porous Mater.* **2016**, *23*, 1269–1278. [CrossRef]

55. Xu, L.; Xiong, Y.; Dang, B.; Ye, Z.; Jin, C.; Sun, Q.; Yu, X. In-situ anchoring of Fe_3O_4/ZIF-67 dodecahedrons in highly compressible wood aerogel with excellent microwave absorption properties. *Mater. Des.* **2019**, *182*, 108006. [CrossRef]

56. Guangli, Y.; Sun, J.; Muhammad, F.; Pengyuan, W.; Zhu, G. Cobalt-based metal organic framework as precursor to achieve superior catalytic activity for aerobic epoxidation of styrene. *RSC Adv.* **2014**, *4*, 38804–38811.

57. Wang, G.; Sun, T.; Sun, Z.; Hu, X. Preparation of copper based metal organic framework materials and its effective adsorptive removal of ceftazidime from aqueous solutions. *Appl. Surf. Sci.* **2020**, *532*, 147411. [CrossRef]

58. Zhao, J.; Gao, F.; Sun, Y.; Fang, W.; Li, X.; Dai, Y. New use for biochar derived from bovine manure for tetracycline removal. *J. Environ. Chem. Eng.* **2021**, *9*, 105585. [CrossRef]

59. Jain, C.K. Adsorption of zinc onto bed sediments of the River Ganga: Adsorption models and kinetics. *Hydrol. Sci. J.* **2001**, *46*, 419–434. [CrossRef]